Energy 347 (2026) 140251

Contents lists available at ScienceDirect

Energy

journal homepage: www.elsevier.com/locate/energy

Vortex-induced vibration piezoelectric energy harvester with arch beam for multi-directional operation and self-powered sensing

Cuipeng Xia [a], Lihua Tang [a,*], Tianle Meng [b], Yawei Wang [c], Huaijun Li [d], Peilun Yin [e], Wan Sun [f], Weiqun Liu [g], Guobiao Hu [c], Kean C. Aw [a]

[a] Department of Mechanical and Mechatronics Engineering, The University of Auckland, Auckland, 1010, New Zealand
[b] Department of Aeronautics, Imperial College London, London, SW7 2AZ, United Kingdom
[c] Internet of Things Thrust, The Hong Kong University of Science and Technology (Guangzhou), Guangzhou, Guangdong, 511400, China
[d] School of Aero Engine, Zhengzhou University of Aeronautics, Zhengzhou, 450015, China
[e] School of Mechatronic Engineering and Automation, Shanghai University, Shanghai, 200444, China
[f] School of Mechanical Engineering, Jiangsu University, Zhenjiang, 212013, China
[g] School of Mechanical Engineering, Southwest Jiaotong University, 610031, Chengdu, China

ARTICLE INFO

Keywords:
Vortex-induced vibration
Piezoelectric energy harvester
Arch beam
Wind direction adaptability
Higher-order vibrational modes
Multiple lock-in ranges

ABSTRACT

Conventional vortex-induced vibration (VIV)-based piezoelectric energy harvesters (PEHs) typically operate effectively only under a single incident wind direction and within a narrow lock-in speed range, resulting in reduced adaptability and efficiency in naturally fluctuating wind conditions. In this study, a VIV-based PEH incorporating an arch beam as a supporting structure is proposed to capture wind energy over a broad range of incident wind directions and multiple lock-in wind speed ranges by activating higher-order vibrational modes. Finite element analysis is first conducted to determine the natural frequencies and corresponding mode shapes of the VIV-based PEHs with both the conventional straight beam and the proposed arch beam configurations. Subsequently, wind tunnel experiments are performed to evaluate the wind energy harvesting performance, including the cut-in wind speed, lock-in wind speed range, incident wind direction range, and electrical output, by leveraging the harvester's multi-modal response. Finally, the superior configuration with a central angle of $3\pi/4$ is selected to demonstrate its application potential, including powering wireless sensors. The results reveal that the proposed harvester can effectively capture wind energy with superior wind direction adaptability and across several lock-in wind speed ranges by activating multiple modes, achieving optimal performance when the second bending mode is excited. Overall, this novel design provides a promising approach for efficiently harvesting wind energy and for powering remote sensing devices under variable natural wind conditions.

1. Introduction

The rapid advancement of technologies such as the Internet of Things (IoT) [1], wearable electronics [2], and environmental monitoring [3] has created increasing demand for sustainable energy supply solutions and advanced self-powered technologies. Conventional battery-powered systems suffer from limited service life and costly replacement, making them unsuitable for long-term, maintenance-free applications [4,5]. As a result, harvesting clean energy from ambient sources, such as tides [6], waves [7], and wind [8,9], to power wireless sensors has emerged as a promising alternative to traditional battery-based approaches [10,11]. Piezoelectric [12–14], electromagnetic [15,16], and triboelectric [17–19] mechanisms are widely adopted energy conversion strategies for transforming ambient clean energy into useable electricity. Among these, the piezoelectric effect has received particular attention owing to its ease of miniaturization and relatively high power density [20,21].

Cantilever beams are widely employed in vibration-based piezoelectric energy harvesters (PEHs) due to their favourable dynamic characteristics, structural simplicity, ease of fabrication, and large deflections [22,23]. However, conventional cantilever-based PEHs suffer from inherent limitations, including non-uniform strain distribution, high resonance frequencies, and narrow operational bandwidths [24–26]. To overcome these drawbacks, researchers have explored PEHs using curved beam structures, which show substantial potential for

* Corresponding author.
E-mail address: l.tang@auckland.ac.nz (L. Tang).

https://doi.org/10.1016/j.energy.2026.140251
Received 26 November 2025; Received in revised form 11 January 2026; Accepted 28 January 2026
Available online 4 February 2026

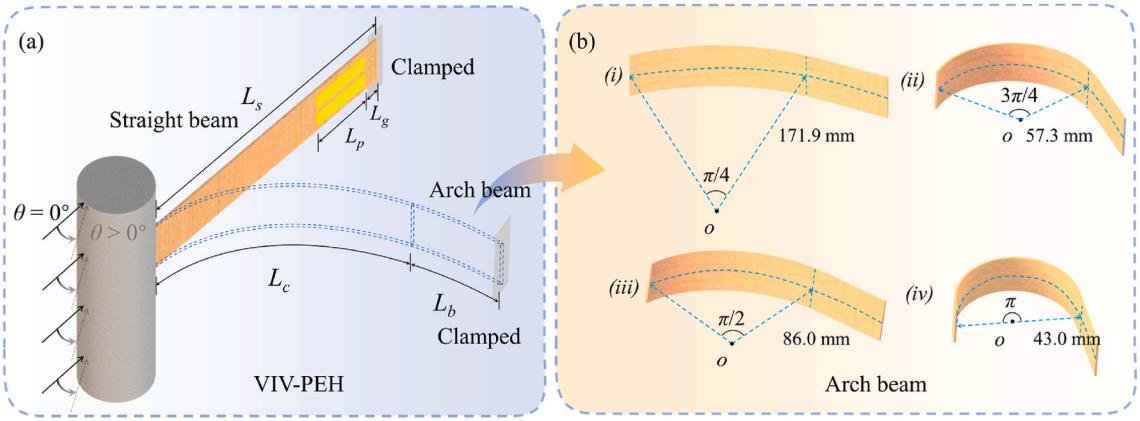

Fig. 1. Schematic of VIV-based piezoelectric energy harvesters with (a) straight beam and proposed arch beam, (b) arch beam with different radii of curvature and corresponding central angles.

improving output performance and expanding practical application scenarios [27–30]. For example, Jung et al. [31] proposed a curved PEH and experimentally demonstrated that a more uniformly distributed stress across the piezoelectric layer results in an enhanced electrical output. Yang et al. [32] introduced a PEH with arc-shaped piezoelectric patches. A finite element simulation revealed that the curved beam structure induces evenly distributed high stress, and experimental results validated its superior power output compared with the counterpart using a straight beam. Subsequently, Zhou et al. [33] developed an analytical model for curved-beam PEHs based on Timoshenko beam theory and the mode expansion method, providing analytical guidance for composite arc-shaped harvesters with variable curvature. Curved supporting structures have been shown to be effective in low-frequency energy harvesting [34,35]. Wang et al. [36] reported a low-frequency curved PEH, where adjusting the radius of curvature enabled matching with the source excitation frequency. Both experimental and numerical results demonstrated its strong low-frequency vibration absorption capacity and enhanced energy harvesting efficiency. Zhang et al. [24] presented a curved pre-bent PEH for harvesting low-frequency vibration energy while mitigating damage from excessive deformation. Their results indicated that the optimal low-frequency bandwidth can be achieved through appropriate tuning of the structural parameters. Recent studies have further shown that introducing geometric/magnetic nonlinearities into PEHs with curved beams can effectively broaden the operational bandwidth and enhance output performance [37–41]. He et al. [42] proposed a low-frequency bistable PEH comprising two curved piezoelectric plates. Both theoretical and experimental results demonstrated that the nonlinear force alters the dynamics of the harvester and broadens its operational bandwidth.

Wind, one of the most abundant renewable energy sources on Earth, has been extensively exploited for energy harvesting by leveraging various aeroelastic instability mechanisms, such as buffeting [43], flutter [44,45], vortex-induced vibration (VIV) [46–49], galloping [50–52], and wake galloping [53,54]. Among these mechanisms, VIV-based energy harvesters have garnered considerable attention due to their superior energy conversion efficiency within a relatively low lock-in wind speed range [55–57]. The performance of VIV-based energy harvesters is highly sensitive to variations in airflow velocity and direction [58], whereas natural wind conditions exhibit temporal fluctuations in both parameters [59]. Consequently, expanding the operational range of wind speed or wind direction is crucial for improving the applicability of VIV-based energy harvesters for practical applications. Boddapati et al. [60] introduced a VIV-based PEH employing a cantilevered bistable composite laminate, which operates in two distinct dynamic modes at room temperature. While theoretical modeling and wind tunnel experiments demonstrated that the harvester can achieve high electrical output within dual lock-in wind speed ranges, its energy harvesting capability is restricted to a single incident wind direction. Chen et al. [61] developed a two-degree-of-freedom VIV-based PEH consisting of two parallel, elastically coupled cylinders. Numerical simulations and experimental investigations demonstrated that this configuration enhances power generation over two lock-in ranges at low wind speeds; however, the energy harvesting performance remains limited to a specific incident wind direction. Jia et al. [62] developed a VIV-based PEH employing an asymmetric cylindrical bluff body to excite dual vibration modes for wind energy harvesting. Despite its capability of multi-modal energy extraction, the harvester's output is restricted by the narrow ranges of effective incident wind directions and lock-in wind speeds. Extensive research has investigated various VIV-based energy harvester configurations to improve their adaptability to different incident wind directions [63–65]. Li et al. [66] proposed an in-plane omnidirectional VIV-based PEH consisting of a cylindrical shell bluff body supported by internal piezoelectric composite beams. Numerical simulations and experimental results revealed that the design enhances directional adaptability within the lock-in wind speed range in the single bending mode. Zhang et al. [67] developed a VIV-based PEH comprising a foam sphere connected with a supporting piezoelectric beam to harvest wind energy from the horizontal direction. While this configuration effectively addresses directional limitations, the harvester operates only within a narrow lock-in wind speed range, extracting energy solely through the bending mode. To achieve an extended lock-in wind speed range with multi-directional capability, Wang et al. [68] and Shi et al. [69] proposed VIV-based PEHs incorporating a cross-coupled dual-beam design. Wind tunnel experiments demonstrated that such a configuration enhances electrical output performance by broadening the lock-in wind speed range and triggering dual bending modes. Su et al. [70] proposed a VIV-based bi-directional PEH comprising a U-shaped beam and a cylindrical bluff body. Experimental results demonstrated that the harvester could capture wind energy from two orthogonal incident directions within dual lock-in wind speed ranges by activating both vertical and horizontal bending vibration modes. Li et al. [71] introduced an omnidirectional VIV-based PEH incorporating a rotating fixed seat and two cylindrical bluff bodies arranged in series. Wind tunnel experiments demonstrated that the system exhibited bistable behaviour with a bending mode being triggered with suitable design parameters.

Although numerous approaches have been developed for VIV-based energy harvesting under different incident wind directions, limited attention has been given to harvesters that can simultaneously achieve multi-directional performance and multiple lock-in wind speed ranges by leveraging higher-order vibrational modes, including both bending and torsional modes. Our preliminary experimental results [57] showed the possibility of using a tri-section beam in a VIV-based PEH to scavenge wind energy, with different vibration modes being activated in

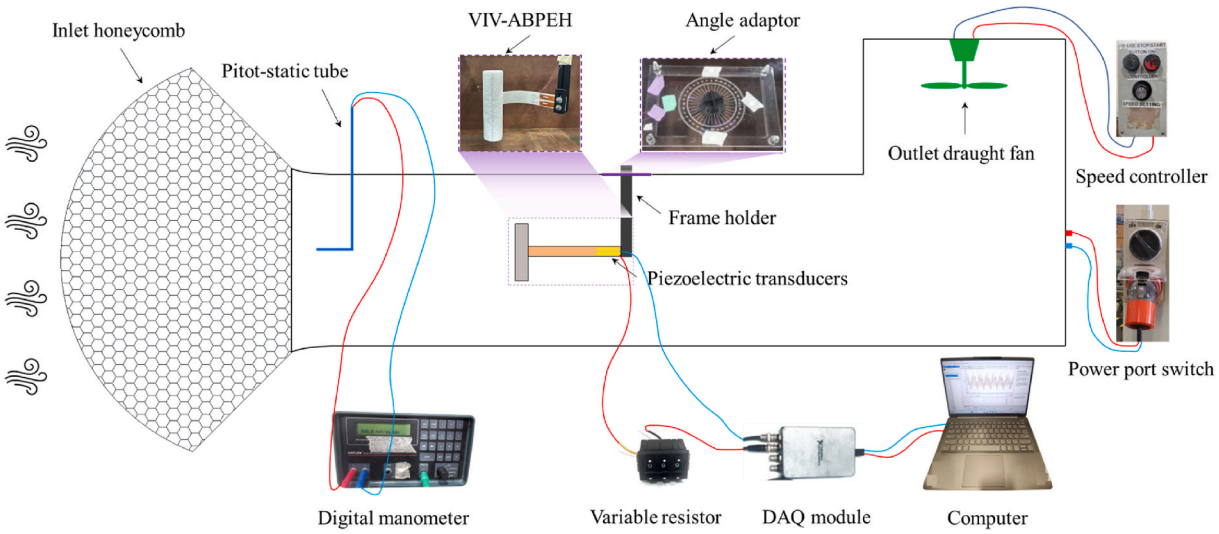

Fig. 2. Experimental setup for wind tunnel test and installation configuration of the VIV-ABPEH.

response to varying wind directions. However, it lacks a comprehensive analysis of the effects of the beam's design parameters. Building on that multi-section beam idea and inspired by the curved beam designs, this study develops a novel VIV-based arch beam piezoelectric energy harvester (VIV-ABPEH). With a properly tuned central angle of the arch beam, the proposed VIV-ABPEH can harness multi-directional wind energy via both bending and torsional modes, covering multiple lock-in wind speed ranges. The performance is comprehensively evaluated using five metrics. The rest of this paper is organized as follows. Section 2 introduces the VIV-ABPEH design, as well as the setups of the finite element analysis (FEA) and wind tunnel experiment. Section 3 presents the experimental results and parametric study of the proposed VIV-ABPEHs with various central angles, emphasizing their wind-directional adaptability and mode activation across multiple lock-in wind speed ranges. Furthermore, the electrical output performance and practical powering applications of the developed harvesters are systematically investigated. Finally, Section 4 summarizes the key findings of this work.

2. Finite element simulation and experimental methodology

The finite element analysis (FEA) and wind tunnel setups for the conventional VIV-based piezoelectric energy harvester with straight beam (VIV-SBPEH) and the proposed VIV-ABPEH with different curvatures are described in this section. Section 2.1 presents the geometrical parameters of the VIV-based PEHs, Section 2.2 details the numerical simulation settings using ANSYS, and Section 2.3 describes the experimental setup.

2.1. Geometric configuration

Fig. 1(a) illustrates the schematic of the vortex-induced vibration-based piezoelectric energy harvesters (VIV-PEHs) employing straight and arch beams, denoted as VIV-SBPEH and VIV-ABPEH, respectively. In both configurations, a cylindrical bluff body with a diameter of $d = 50$ mm and a height of $h = 140$ mm is attached at the free end of the beam, while piezoelectric patches are bonded near the clamped end. The VIV-SBPEH consists of a straight beam with a length of $L_s = 180$, where the two piezoelectric patches (Macro Fiber Composite-MFC, Smart Material Corp.) have a length of $L_p = 37$ mm, and the gap between the clamped end and the piezo-patch's edge is $L_g = 8$ mm. The beam of the proposed VIV-ABPEH comprises two segments: a curved section with a length of $L_c = 135$ mm and a straight section with a length of $L_b = L_p + L_g$. As illustrated in Fig. 1(b), four radii of curvature (171.9 mm, 86.0 mm, 57.3 mm, and 43.0 mm) corresponding to central angles of $\pi/4$, $\pi/2$, $3\pi/4$, and π, respectively, are considered to investigate the effect of curvature of the arch beam on the output performance of the proposed VIV-ABPEH.

2.2. Modal analysis

To investigate the natural frequencies and mode shapes of the traditional VIV-SBPEH and the proposed VIV-ABPEH, FEA is carried out in ANSYS Workbench. To accurately capture the three-dimensional dynamic behaviour of the system, solid elements are used for all components, including the beam, piezoelectric transducers, and cylindrical bluff body. A structured mesh comprising HEX8 elements is applied to the beam and piezoelectric transducers, as their simple geometry facilitates computational efficiency and fast convergence. An unstructured mesh consisting of TET10 elements is applied to the cylindrical bluff body to accommodate its geometric complexity and ensure higher mesh quality and simulation accuracy. A mesh size of 0.005 m is adopted to achieve a balance between computational cost and solution accuracy in the modal analysis. This meshing strategy for the VIV-SBPEH resulted in a total of 3571 solid elements, comprising 3299 TET10 elements and 272 HEX8 elements. For the VIV-ABPEH configurations with central angles of $\pi/4$, $\pi/2$, $3\pi/4$, and π, the corresponding total numbers of solid elements are 3823, 3817, 3823, and 3973, respectively, including 3299, 3299, 3299, and 3455 TET10 elements, along with 524, 518, 524, and 518 HEX8 elements. The FEA results of the natural frequencies and corresponding mode shapes for the VIV-SBPEH and VIV-ABPEHs with different central angles are presented in the Supplementary Materials.

2.3. Experimental setup

Fig. 2 shows the prototype of the VIV-ABPEHs and the experimental setup used for the wind tunnel test. The aerodynamic tests are conducted in an open-loop wind tunnel, where the incident wind direction on the harvester is adjusted using an angle adapter mounted at the top of the test section. The adapter scale, fabricated via laser cutting, allowed accurate monitoring of the wind direction. The harvester consists of an arch beam with various curvature radii bonded with MFCs (capacitance $C_p = 15.5$ nF) and a cylindrical bluff body attached at the free end. The beam is clamped by a rigid frame holder, ensuring accurate alignment and stable positioning within the test section. The airflow is generated by an outlet draught fan, while a honeycomb structure installed at the inlet straightens and stabilizes the flow. Wind speed is measured in real-time using a pitot-static tube, and the incident airflow is regulated by a

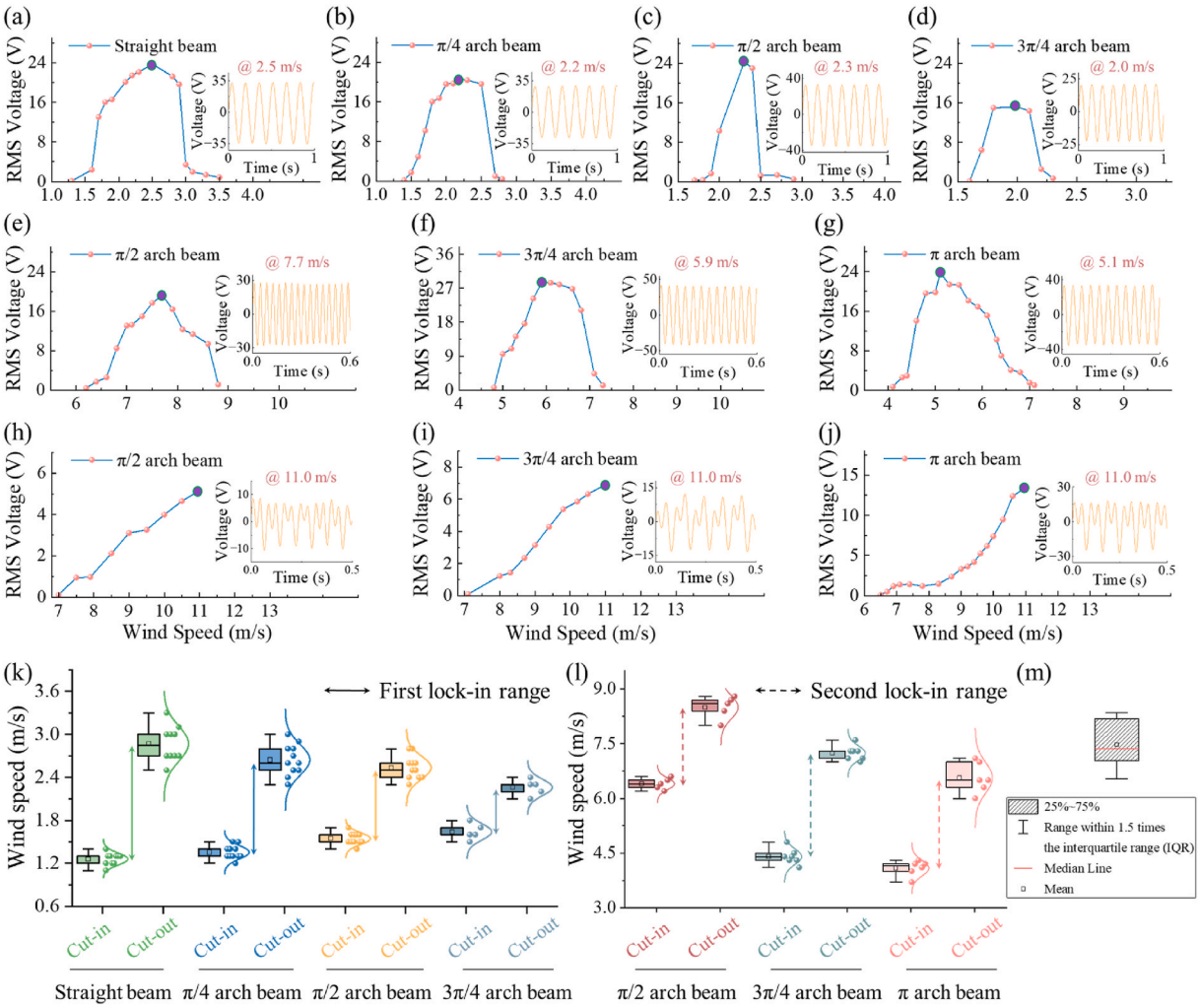

Fig. 3. RMS voltage output of V_{L1} of the VIV-SBPEH and VIV-ABPEHs with different central angles in different wind speed ranges and incident wind directions from experiment: (a) VIV-SBPEH in the 1st order bending mode at $\theta = 0°$; VIV-ABPEHs in the 1st order bending mode with (b) central angle of $\pi/4$ at $\theta = 10°$, (c) central angle $\pi/2$ at $\theta = 190°$, (d) central angle $3\pi/4$ at $\theta = 200°$; VIV-ABPEHs in the 2nd order bending mode with (e) central angle $\pi/2$ at $\theta = 140°$, (f) central angle $3\pi/4$ at $\theta = 150°$, and (g) central angle π at $\theta = 190°$; VIV-ABPEHs in the 1st and 2nd order coupled torsional modes with (h) central angle $\pi/2$ at $\theta = 200°$, (i) central angle $3\pi/4$ at $\theta = 40°$, (j) central angle π at $\theta = 40°$; statistical lock-in ranges for the harvesters showing (k) the 1st lock-in range and (l) the 2nd lock-in range; (m) schematic illustration of the box-error plot.

variable-speed controller. The electrical outputs of the VIV-SBPEH and VIV-ABPEHs with different central angles are measured by a data acquisition (DAQ) module (NI 9229, National Instruments) with an internal resistance of $R_{DAQ} = 1$ MΩ. A large resistor ($R = 10$ MΩ) is connected in series with the DAQ module, resulting in a total external load resistance $R_{L1} = R_{DAQ} + R$. The voltage V_{L1} across this load can be determined using the voltage divider rule.

3. Results and discussion

This section provides a detailed comparison between the VIV-SBPEH and VIV-ABPEHs based on five performance metrics: cut-in wind speed, lock-in wind speed ranges, mode activation, wind direction adaptability, and electrical power output. The harvester exhibiting superior performance across these criteria is subsequently selected for demonstration, including the application of wireless sensing.

3.1. Cut-in wind speed and lock-in ranges

The lock-in phenomenon, also referred to as vortex shedding synchronization, occurs when the frequency of vortex shedding in the airflow matches the natural frequency of the vibrating structure. Specifically, the cut-in speed denotes the onset wind speed at which structural vibrations become sufficiently excited to trigger the lock-in condition, while the cut-out speed indicates the wind speed at which the harvester stops functioning. Notably, a VIV-PEH can realize significantly improved energy harvesting performance when operating within the lock-in wind speed range.

Fig. 3 shows the cut-in wind speeds and lock-in ranges of the conventional VIV-SBPEH and the proposed VIV-ABPEHs with different central angles under different incident wind directions in the experiment, indicated by the root-mean-square (RMS) voltage output of V_{L1}. The reference orientation (zero-incident direction, $\theta = 0°$ as shown in Fig. 1) is defined along the axis parallel to the straight beam or tangent to the arch beam on which the cylindrical bluff body is mounted, with positive θ indicating wind directions measured counter-clockwise from the top view of the harvester. Both the VIV-SBPEH and the VIV-ABPEHs with the central angles of $\pi/4$, $\pi/2$, and $3\pi/4$ are capable of harvesting wind energy within the 1st lock-in wind speed range (Fig. 3(a)–(d)) through the excitation of the 1st order bending mode. Furthermore, the proposed VIV-ABPEHs with central angles of $\pi/2$, $3\pi/4$, and π can capture wind energy within higher lock-in wind speed ranges (Fig. 3(e)–(g)) when the 2nd order bending mode is activated. In addition to harvesting wind energy through the activation of bending modes, the proposed

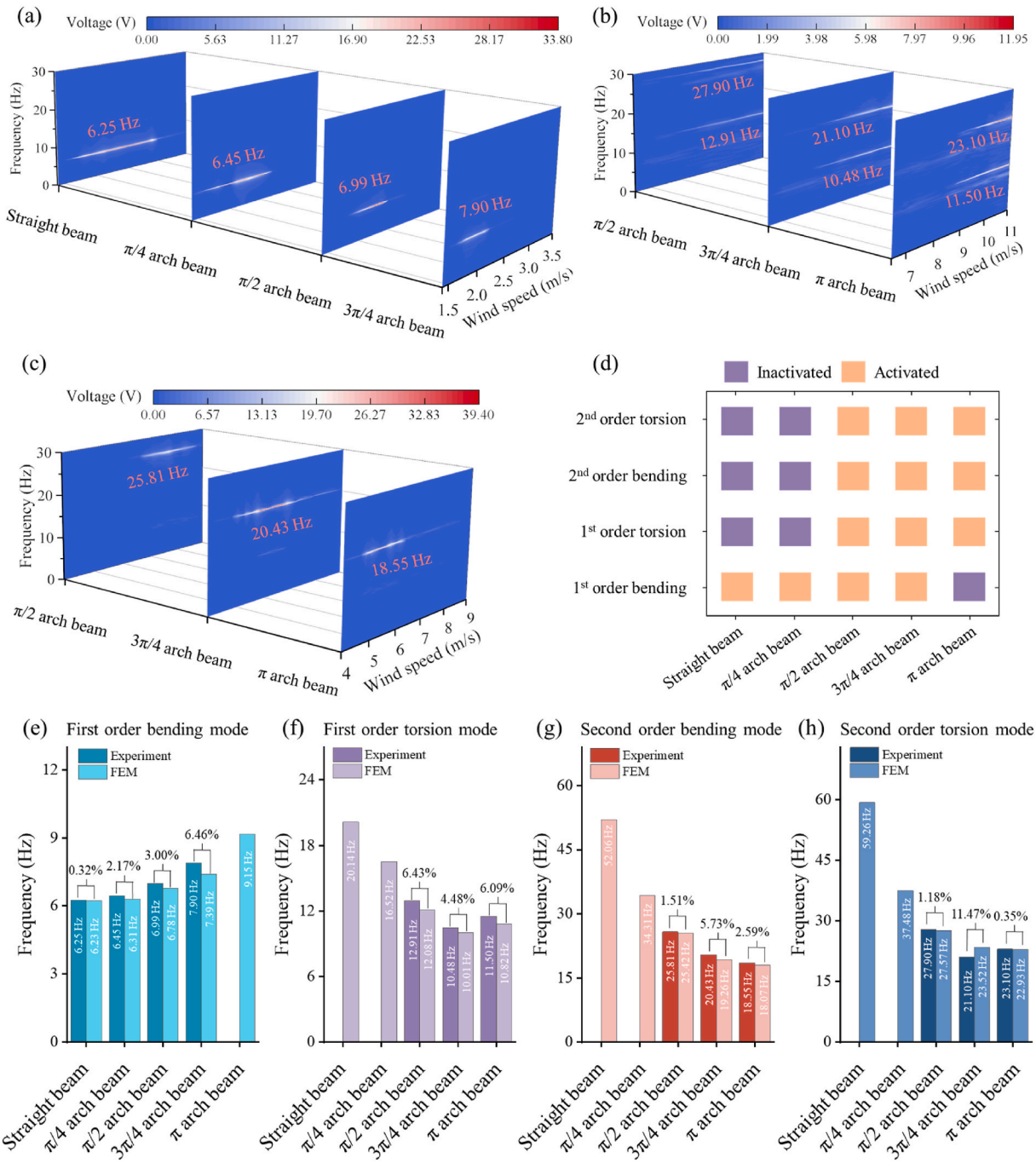

Fig. 4. Mode activation of the VIV-SBPEH and VIV-ABPEHs across different wind speeds: (a) 1st order bending mode for the VIV-SBPEH and VIV-ABPEHs with central angles of π/4, π/2, and 3π/4; (b) 1st and 2nd order torsional modes for VIV-ABPEHs with central angles of π/2, 3π/4, and π; (c) 2nd order bending mode for VIV-ABPEHs with central angles of π/2, 3π/4, and π; and (d) Activated and inactivated modes of the VIV-SBPEH and VIV-ABPEHs (see Supplementary Videos S1-S3 for the activation of the first four modes of the VIV-ABPEH with central angle of 3π/4). Comparison of natural frequencies between experimental results and FEA predictions for the VIV-SBPEH and VIV-ABPEHs of the first four modes: (e) 1st order bending, (f) 1st order torsional, (g) 2nd order bending, and (h) 2nd order torsional modes.

VIV-ABPEHs with the central angles of π/2, 3π/4, and π are also capable of exciting the 1st and 2nd order coupled torsional modes to extract wind energy, as illustrated in Fig. 3(h)–(j). However, the VIV-ABPEH with a central angle of π arch beam fails to excite the 1st order bending mode, whereas both the VIV-SBPEH and VIV-ABPEH with a central angle of π/4 are unable to activate the 1st and 2nd order torsional modes as well as the 2nd order bending mode for wind energy harvesting. These observations can be attributed to the higher natural frequencies associated with the corresponding vibrational modes, and a detailed discussion on mode activation is presented in Section 3.2. Fig. 3 (k) and (l) show the statistical results of the cut-in and cut-out wind speeds for the VIV-SBPEH and VIV-ABPEHs. The data points are collected at different incident wind directions. For each harvester configuration, wind tunnel tests are conducted over the full range of wind directions (ranging from 0° to 360°), and at each direction, the corresponding cut-in and cut-out wind speeds associated with the excitation of the 1st order bending mode (Fig. 3(k)) or 2nd order bending mode (Fig. 3(l)) are measured. The box-error plots summarize the

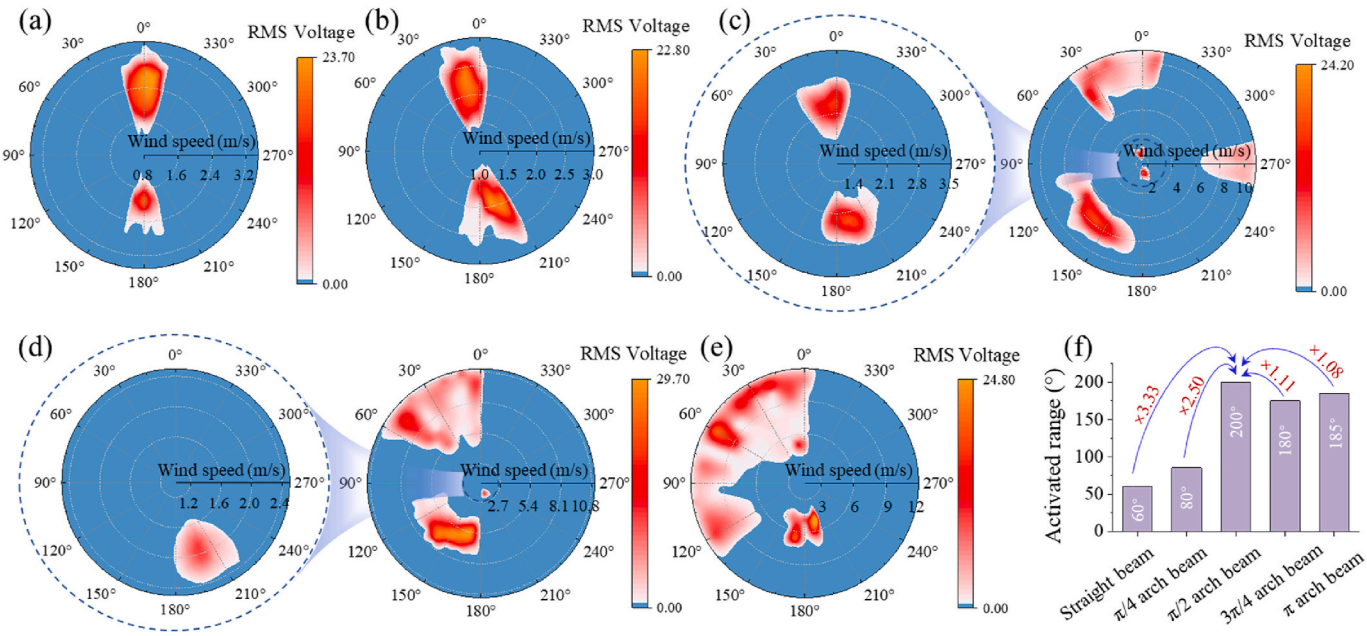

Fig. 5. Wind directional adaptability of the conventional VIV-SBPEH (a) and proposed VIV-ABPEHs with different central angles: (b) π/4, (c) π/2, (d) 3π/4, and (e) π. (f) Comparison of activated wind direction ranges of the VIV-SBPEH and VIV-ABPEHs.

statistical characteristics of these datasets, including the interquartile range, median, and mean, as illustrated in Fig. 3(m). The accompanying smooth curves represent the overall distribution of the measured values, which is assumed to be approximately a normal (Gaussian) distribution. These curves are not analytical fits to wind-speed trends, but rather serve to visualize the distributions of cut-in and cut-out wind speeds, central tendency, and dispersion of the experimental data aggregated over the full range of wind directions. Based on these analyses, the arithmetic mean values of the cut-in and cut-out wind speeds are extracted and used to define the lock-in wind-speed ranges for the 1st and 2nd order bending modes, calculated as the difference between the mean cut-out and cut-in speeds. As illustrated in Fig. 3(k), when the 1st order bending mode is activated, the arithmetic mean cut-in wind speeds for the VIV-SBPEH and the VIV-ABPEHs with central angles of π/4, π/2, and 3π/4 are 1.28 m/s, 1.36 m/s, 1.55 m/s, and 1.64 m/s, respectively, while their corresponding arithmetic mean cut-out wind speeds are 2.87 m/s, 2.65 m/s, 2.54 m/s, and 2.26 m/s. Consequently, the 1st lock-in wind speed ranges are calculated as 1.59 m/s, 1.29 m/s, 0.99 m/s, and 0.62 m/s. For the 2nd order bending mode, shown in Fig. 3(l), the VIV-ABPEHs with central angles of π/2, 3π/4, and π exhibit larger arithmetic mean cut-in and cut-out wind speeds. Specifically, the arithmetic mean cut-in wind speeds are 6.40 m/s, 4.40 m/s, and 4.08 m/s, with corresponding arithmetic mean cut-out speeds of 8.50 m/s, 7.24 m/s, and 6.57 m/s, resulting in 2nd lock-in speed ranges of 2.10 m/s, 2.84 m/s, and 2.49 m/s. To quantify the overall wind-speed adaptability, the comprehensive lock-in range is defined as the union of the lock-in intervals of the 1st and 2nd order bending modes. When the two bending mode lock-in ranges do not overlap, the comprehensive range is obtained by summing the individual lock-in ranges. Therefore, the proposed VIV-ABPEH with a central angle of 3π/4 demonstrates the widest comprehensive lock-in range of 3.46 m/s, attributed to the combined activation of both the 1st and 2nd lock-in regions. By contrast, the comprehensive lock-in range of the VIV-SBPEH and the VIV-ABPEHs with central angles of π/4, π/2, and π are comparatively narrower, with values of 1.59 m/s, 1.29 m/s, 3.09 m/s, and 2.49 m/s.

3.2. Mode activation

During the VIV lock-in range, the vortex shedding frequency adaptively synchronizes with the coupled fluid-structure dynamics through a wake-capture mechanism [72]. Although the VIV response remains narrow-banded, the vibration frequency exhibits a slight drift with increasing reduced velocity due to the variation in the effective added mass [73,74]. This drift arises from the evolving phase relationship between the fluid forcing and the structural response [75], which modifies the apparent inertia of the system and enables sustained synchronization over a finite lock-in bandwidth. During the wind tunnel experiments, the steady-state voltage signals corresponding to each activated vibration mode are measured and subsequently analysed in the frequency domain by Fast Fourier Transform (FFT). The dominant peak in the frequency spectrum is identified as the vibration frequency of the corresponding mode. Accordingly, the mean value of the experimentally measured vibration frequencies within the lock-in range is adopted as the representative frequency of the corresponding vibration mode for the VIV-ABPEH.

Fig. 4 illustrates the mode activation of the VIV-SBPEH and VIV-ABPEHs. Compared with the conventional VIV-SBPEH, the proposed VIV-ABPEHs demonstrate enhanced output performance through the excitation of multiple vibrational modes. Specifically, as shown in Fig. 4 (a), both the traditional VIV-SBPEH and the VIV-ABPEHs with central angles of π/4, π/2, and 3π/4 can harvest wind energy via the 1st order bending mode, with corresponding frequencies of 6.25 Hz, 6.45 Hz, 6.99 Hz, and 7.90 Hz, respectively. Moreover, higher order vibrational modes (including the 1st and 2nd order coupled torsional modes, the 2nd order bending mode) are experimentally observed for the VIV-ABPEHs with central angles of π/2, 3π/4, and π, as shown in Fig. 4(b) and (c), The corresponding frequencies are 12.91 Hz, 10.48 Hz, and 11.50 Hz for the 1st order torsional mode; 27.90 Hz, 21.10 Hz, and 23.10 Hz for the 2nd order torsional mode; and 25.81 Hz, 20.43 Hz, and 18.55 Hz for the 2nd order bending mode. These modes are absent in the VIV-SBPEH and VIV-ABPEH with the central angle of π/4. The working mechanism of the 1st and 2nd order coupled torsional modes can be attributed to geometry-induced modal coupling and nonlinear internal resonance. The arch-beam geometry inherently promotes coupling between the fundamental and higher-order torsional deformations, while oblique incident wind direction generates unsteady aerodynamic moments with broadband frequency content. When the flow excitation frequency approaches either the 1st or 2nd order torsional natural

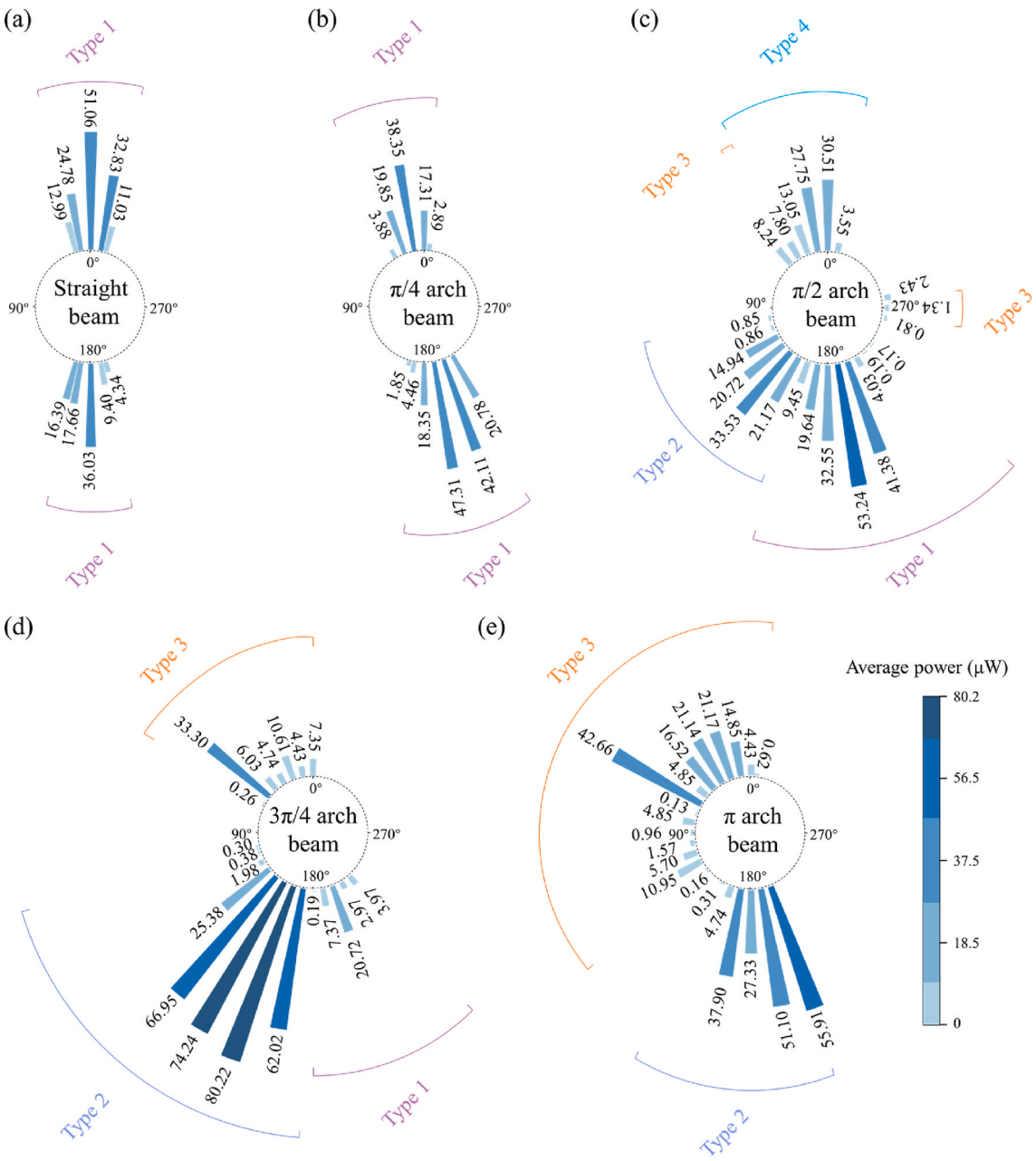

Fig. 6. Average output power P_{L1} for the VIV-SBPEH (a) and VIV-ABPEHs with different central angles: (b) π/4, (c) π/2, (d) 3π/4, and (e) π.

frequency, an initial torsional oscillation is triggered. As the vibration amplitude increases, nonlinear modal interactions enable energy transfer between the two torsional modes, resulting in their coexistence or alternating dominance. Fig. 4(d) presents the activated and inactivated vibrational modes for the traditional VIV-SBPEH and the proposed VIV-ABPEHs. It can be observed that the VIV-ABPEHs with central angles of π/2 and 3π/4 exhibit superior energy-harvesting performance, as they can activate the first four vibrational modes for wind energy extraction (see Supplementary Videos S1-S3 for the mode activation of the 3π/4 configuration). In contrast, both the VIV-SBPEH and the VIV-ABPEH with a central angle of π/4 can only excite the fundamental bending mode, and the VIV-ABPEH with a central angle of π cannot excite the 1st order bending mode. FEA is employed to predict the natural frequencies and vibrational modes of the VIV-SBPEH and VIV-ABPEHs, showing good agreement with the experimentally measured frequencies of the activated modes (Fig. 4(e)-4(h)). Specifically, under the 1st order torsional mode, the frequency deviations between the experimental results and FEA predictions for the VIV-ABPEHs with central angles of π/2, 3π/4, and π are 6.43%, 4.48%, and 6.09%, respectively. For the 2nd order bending mode, the corresponding deviations are 1.51%, 5.73%, and 2.59%, respectively. Higher order vibrational modes for the VIV-SBPEH and VIV-ABPEH with a central angle of π/4 are not observed in the wind tunnel test because of their relatively high natural frequencies (20.14 Hz for VIV-SBPEH and 16.52 Hz for VIV-ABPEH with the central angle of π/4 in the 1st order torsional mode, 52.06 Hz and 34.1 Hz in the 2nd order bending mode, and 59.26 Hz and 37.48 Hz under the 2nd order torsional mode, respectively).

3.3. Wind direction adaptability

Fig. 5 presents a comprehensive comparison of the wind directional adaptability between the conventional VIV-SBPEH and the proposed VIV-ABPEHs with various central angles, indicated by the RMS voltage output of V_{L1}. The embedded radial scale lines indicate the wind speed

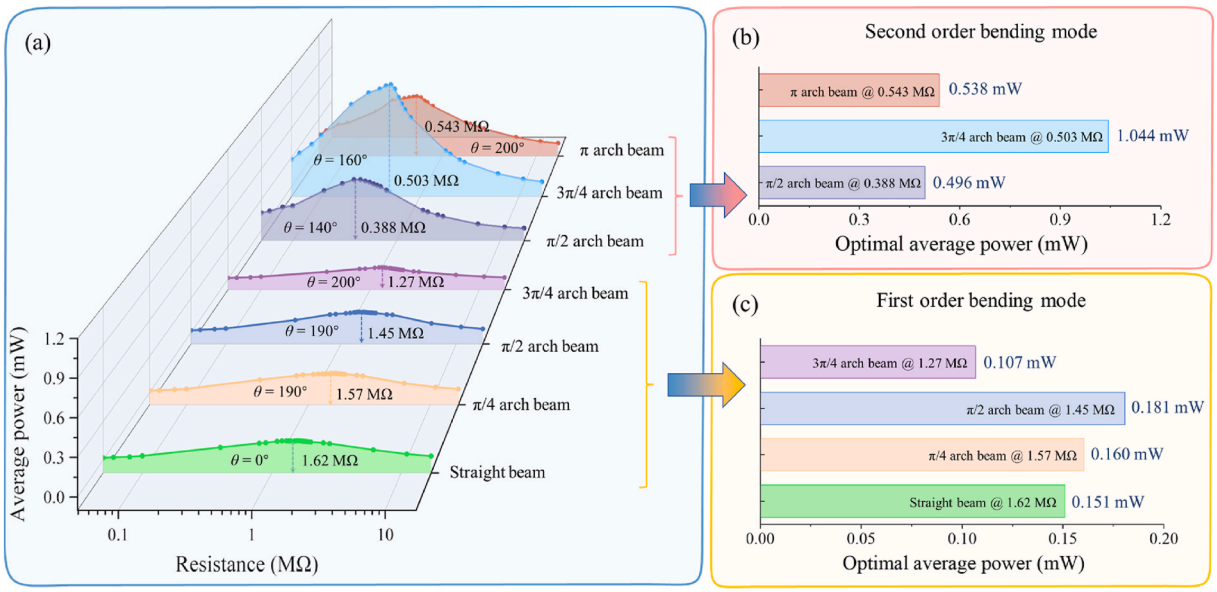

Fig. 7. Power output performance for the VIV-SBPEH and VIV-ABPEHs: (a) average power output P_{L2} for the harvesters with varying resistance, (b) optimal power output for the VIV-ABPEHs with central angles of π/2, 3π/4, and π in the 2nd order bending mode, and (c) optimal power outputs for the VIV-SBPEH and VIV-ABPEHs with central angles of π/4, π/2, and 3π/4 in the 1st order bending mode.

magnitude (m/s) corresponding to the RMS voltage responses at each incident wind direction. To determine the activation ranges of the VIV-based harvester, wind tunnel experiments are conducted by rotating the harvester prototype from 0° to 360° at 5° intervals. Near the transition boundaries between activation and inactivation, finer angular adjustments are made with a 1° interval. Vortex-induced vibration is triggered when the measured voltage signal exhibits a steady-state periodic response. As illustrated in Fig. 5(a), the traditional VIV-SBPEH is capable of harvesting wind energy when the wind direction falls within 0°-15°, 165°-195°, and 345°-360°, resulting in a total activated incident wind direction range of 60°. By contrast, the VIV-ABPEH with a central angle of π/4 demonstrates an expanded activated range of 0°-30°, 165°-210°, and 355°-360°, yielding a total activated wind direction range of 80° (Fig. 5(b)). The configuration with a central angle of π/2 demonstrates superior adaptability with an activated incident wind direction of 200° across 0°-40°, 100°-230°, 260°-280°, and 350°-360° (Fig. 5(c)). Similarly, the VIV-ABPEH with a central angle of 3π/4 achieves a broad activated range of 180°, covering 0°-65° and 105°-220° (Fig. 5(d)). In addition, the configuration with a central angle of π attains an extensive activated range of 185°, spanning 0°-130°, 148°-198°, and 355°-360° (Fig. 5(e)). The experimental results, summarized in Fig. 5(f), clearly demonstrate that the proposed VIV-ABPEHs with different central angles exhibit significantly improved directional adaptability compared to the conventional VIV-SBPEH, with the configuration of a central angle of π/2 achieving the broadest activated directional range. Among them, the configuration of π/2 achieves the broadest activated directional range of 200°, which is 2.50 times that of the configuration of π/4 (80°), 1.11 times that of the 3π/4 configuration (180°), 1.08 times that of the configuration of π (185°), and 3.33 times that of the conventional VIV-SBPEH (60°). The observed expansion of the activated wind-direction range can be attributed to the combined contribution of bending and torsional vibration modes. For bending-dominated responses, efficient energy extraction occurs when the wind-induced excitation (aerodynamic lift force) direction is aligned with the bending direction. In contrast, torsional modes are excited by aerodynamic moments arising from asymmetric pressure distributions on the bluff body, particularly when geometric asymmetry is introduced by the arch-beam configuration. Consequently, the combination of bending and torsional oscillations enables sustained electrical power generation in different wind directions, broadening the effective wind-direction operating range.

3.4. Power output performance

Based on the RMS value of V_{L1}, V_{L1rms}, the average output power is then calculated as $P_{L1} = V_{L1rms}^2/R_{L1}$. Fig. 6 illustrates the electrical power output P_{L1} of the VIV-SBPEH and VIV-ABPEHs with different central angles, evaluated under their corresponding activated modes. For clarity, the vibration modes are categorized as follows: the 1st order bending mode is referred to as Type 1, the 2nd order bending mode as Type 2, the 1st and 2nd order torsional coupled modes as Type 3, and the 1st order bending mode together with 1st and 2nd order torsional coupled modes with varying wind speed as Type 4. As shown in Fig. 6(a) and (b), both the traditional VIV-SBPEH and the VIV-ABPEH with a central angle of π/4 can extract wind energy through activation of the 1st order bending mode (Type 1) across their activated incident wind direction ranges. It is noteworthy that the conventional straight-beam harvester and the π/4 configuration achieve relatively high average output powers of 51.06 μW and 47.31 μW, respectively, at incident wind directions of 0° and 190°. The VIV-ABPEH with a central angle of π/2 (Fig. 6(c)) exhibits the capability to harvest wind energy through multiple vibration modes over a broad range of incident wind directions. Specifically, Type 1 is observed between 170° and 230°, while Type 2 is activated in the incident wind direction range of 100° to 169°. The Type 3 occurs within the ranges of 31°-40° and 260°-280°, respectively. Additionally, Type 4 is identified within the ranges of 350°-360° and 0°-30°. In these conditions, the harvester achieves peak average output powers of 53.24 μW and 33.53 μW for Type 1 and Type 2, corresponding to incident wind directions of 190° and 140°, respectively. Similarly, the VIV-ABPEH with a central angle of 3π/4 (Fig. 6(d)) also demonstrates the activation of multiple vibration modes, thereby enabling efficient wind energy harvesting over a wide range of incident wind directions. Specifically, Type 1 occurs between 180° and 220°, Type 2 between 105° and 179°, and Type 3 between 0° and 65°. In these conditions, the harvester achieves notable average output powers of 20.72 μW and 80.22 μW for Type 1 and Type 2 responses, respectively, at incident wind directions of 200° and 160°. For the VIV-ABPEH with a central angle of π (Fig. 6(e)), Type 2 is activated within 148°-198°, and Type 3 is triggered across 0°-130° and 355°-360°. The maximum average output power reaches 55.91 μW for the Type 2 response at an incident wind direction of 200°, which is higher than that achieved by the Type 3 response (42.66 μW) at 60°.

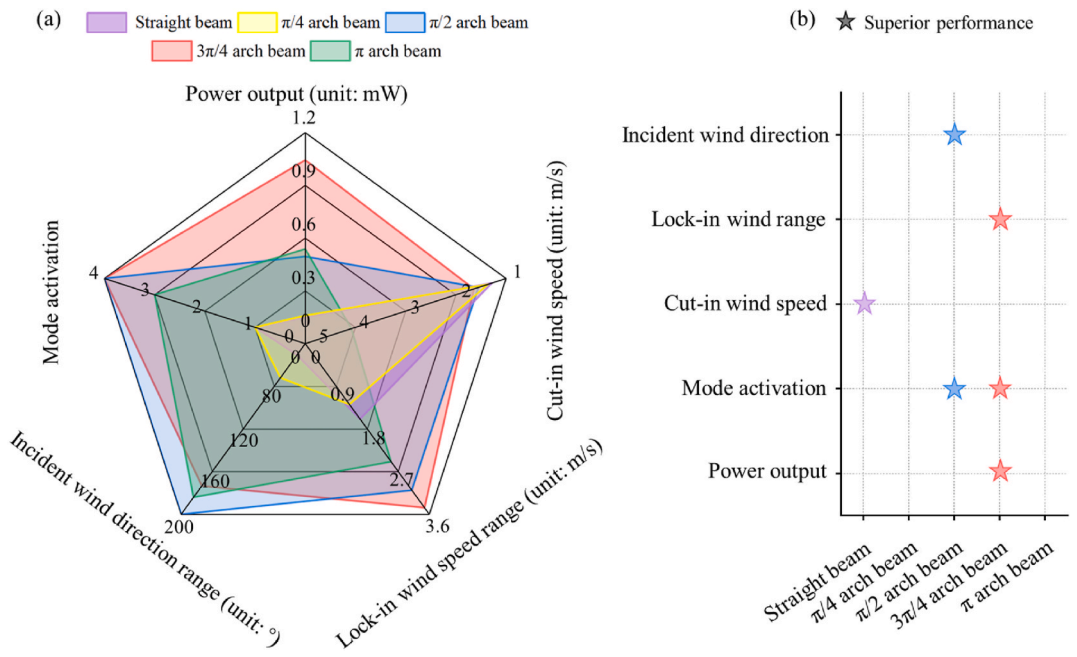

Fig. 8. Comprehensive evaluation of the traditional VIV-SBPEH and VIV-ABPEHs with different central angles: (a) radar map illustrating multi-metric analysis, and (b) comparison of superior performance across the five evaluated metrics.

The VIV-SBPEH and VIV-ABPEH can excite the bending mode to harvest wind energy. As shown in Figs. 5 and 6, the VIV-ABPEHs with central angles of π/2, 3π/4, and π exhibit higher electrical output performance in the bending mode than in the torsional modes. Therefore, the bending modes are selected to evaluate and compare the optimal average power output of the VIV-SBPEH and VIV-ABPEHs. The DAQ module (NI 9229) is used to measure the voltage V_0 across a small resistor R_0 = 50 kΩ. The combined resistance of R_{DAQ} and R_0 can be approximated as R_0 in parallel, which is then connected in series with a variable resistor R_V (ranging from 1 kΩ to 999 kΩ) composed of multiple resistors. The voltage V_{L2} across the overall external load $R_{L2} = R_V + R_0$ is calculated using the voltage divider rule. Based on the RMS values of V_{L2}, V_{L2rms}, the average output power is evaluated as $P_{L2} = V^2_{L2rms}/R_{L2}$, and the maximum power output is obtained by adjusting the variable resistor R_V. Fig. 7 presents a comparison of the electrical power output between the VIV-SBPEH and VIV-ABPEHs with different central angles in the 1st and 2nd order bending modes. To comprehensively evaluate the maximum power output, representative incident wind directions and speeds are selected based on Fig. 6. For the 1st order bending mode, the examined conditions are $\theta = 0°$ at 2.4 m/s for the VIV-SBPEH, $\theta = 190°$ at 2.0 m/s for the VIV-ABPEH with the central angle of π/4, $\theta = 190°$ at 2.0 m/s for the VIV-ABPEH with π/2, and $\theta = 200°$ at 2.0 m/s for the VIV-ABPEH with 3π/4. For the 2nd order bending mode, the conditions are $\theta = 140°$ at 8.2 m/s for the VIV-ABPEH with π/2, $\theta = 160°$ at 6.5 m/s for the VIV-ABPEH with 3π/4, and $\theta = 200°$ at 5.5 m/s for the VIV-ABPEH with π. As shown in Fig. 7(a) and (c), the average power outputs of the VIV-SBPEH and VIV-ABPEHs with central angles of π/4, π/2, and 3π/4 reach peak values of 0.151 mW, 0.160 mW, 0.181 mW, and 0.107 mW, respectively, corresponding to optimal resistances of 1.62 MΩ, 1.57 MΩ, 1.45 MΩ, and 1.27 MΩ. Moreover, the proposed VIV-ABPEHs exhibit generally higher maximum power outputs in the 2nd order bending mode than under the 1st order mode, as illustrated in Fig. 7(b) and (c). In particular, the VIV-ABPEH with a central angle of 3π/4 attains the highest power output of 1.044 mW at an optimal resistance of 0.503 MΩ, outperforming both the configuration of π (0.538 mW at 0.543 MΩ) and the configuration of π/2 (0.496 mW at 0.388 MΩ). These results indicate that the activation of the 2nd order bending mode, particularly for the 3π/4 central angle, can achieve substantial energy harvesting efficiency for the proposed VIV-ABPEHs.

3.5. Performance comparison

For a comprehensive evaluation of the VIV-SBPEH and VIV-ABPEHs with different central angles, five key performance metrics (power output, mode activation, cut-in wind speed, lock-in wind speed range, and incident wind direction range) are employed. As illustrated in Fig. 8 (a), the radar map shows that the VIV-ABPEH with a central angle of 3π/4 achieves the broadest overall coverage, followed by the configurations of π/2 and π, whereas the π/4 configuration and VIV-SBPEH exhibit comparatively smaller coverage areas. The broader coverage of the 3π/4 configuration reflects its superior performance across the evaluated metrics. Specifically, as shown in Fig. 8(b), the 3π/4 configuration achieves the broadest lock-in wind speed range and highest power output, with respective values of 3.46 m/s and 1.044 mW, corresponding to a mass power density of 61.63 μW/g and a volume power density of 3.69 μW/cm^3. Both the 3π/4 and π/2 configurations demonstrate superior mode activation capability, exciting the 1st and 2nd order bending modes as well as the 1st and 2nd order torsional modes, compared with the other harvesters. Additionally, the π/2 configuration exhibits favourable performance over a broader range of incident wind direction, achieving the value of 200°. The VIV-SBPEH, however, outperforms the VIV-ABPEHs in terms of cut-in wind speed (1.28 m/s), which can be attributed to its lowest fundamental natural frequency. Overall, the VIV-ABPEH with a central angle of 3π/4 exhibits the highest performance among all configurations, outperforming others in power output, lock-in wind speed, and mode activation, while maintaining competitive performance in terms of incident wind direction and cut-in wind speed.

3.6. Application demonstration

The VIV-ABPEH with a central angle of 3π/4, identified in Section 3.5 as the optimal configuration, is selected to evaluate the electrical output performance of the harvester working in the 1st and 2nd order bending modes. Wind tunnel tests are conducted to demonstrate its strong potential for practical application, including charging capacitors, lighting LED arrays, and powering wireless sensors, as shown in Fig. 9. In these tests, the prototype is excited under different vibrational modes: the 1st order bending mode is triggered at an incident wind direction of

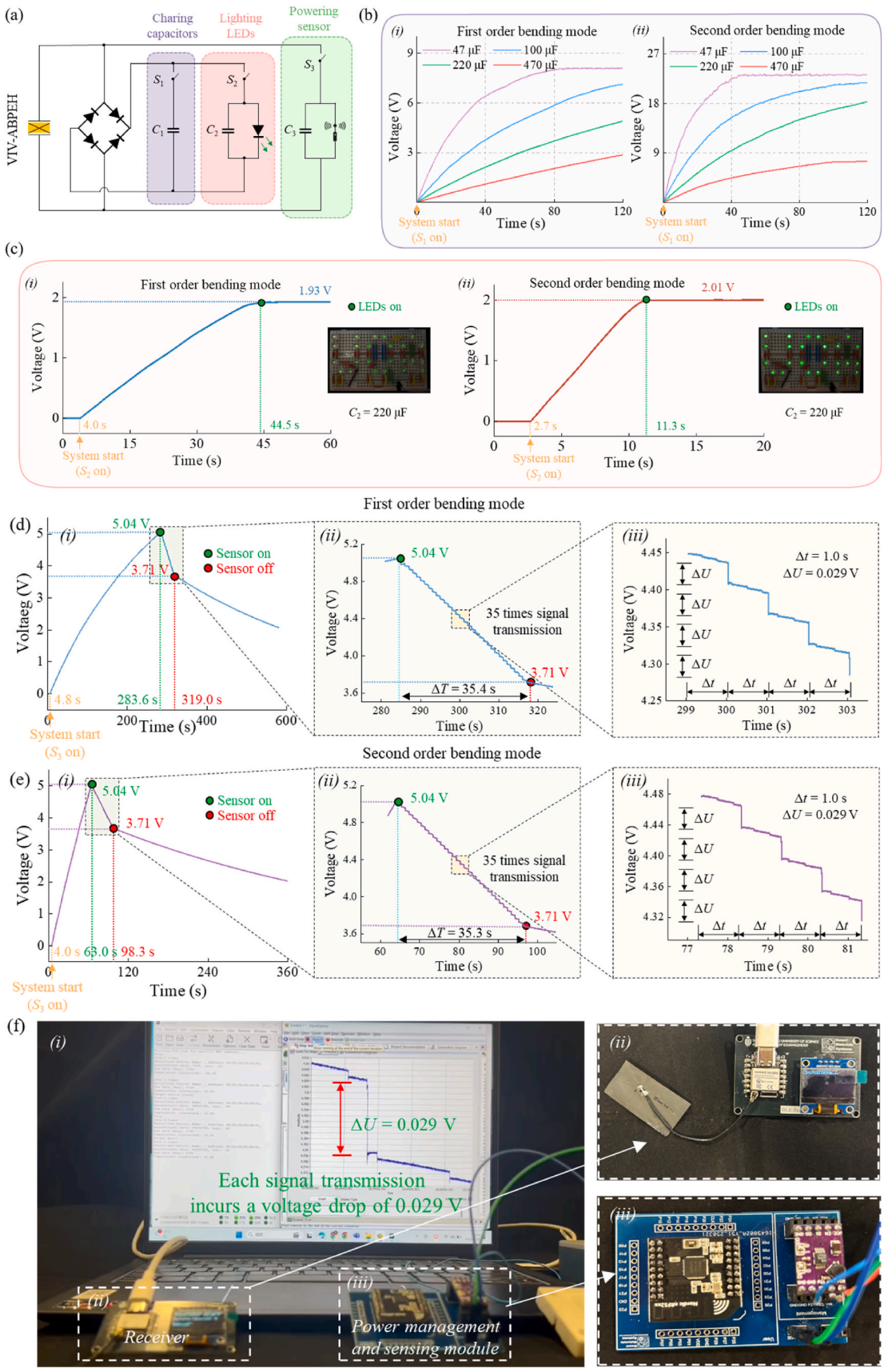

Fig. 9. Application demonstration: (a) circuit connections in various tests; (b) charging capacitors and (c) lighting LED array in the 1st and 2nd order bending modes (Supplementary Videos S4 and S5); Powering wireless temperature sensor (d) in the 1st order bending mode (Supplementary Video S6) and (e) in the 2nd order bending mode (Supplementary Video S7); (f) example of signal transmission (i), receiver (ii) and sensing & transmitting module (iii).

200° with a wind speed of 2.0 m/s, whereas the 2nd order bending mode is triggered at an incident wind direction of 160° with a wind speed of 6.0 m/s. The rectifier in Fig. 9(a) is W10G-237H with a forward voltage of 1 V.

The performance of the proposed 3π/4 configuration in the 1st and 2nd order bending modes is first evaluated by charging a series of capacitors, C_1 (47 μF, 100 μF, 220 μF, and 470 μF), each with a rated voltage of 50 V (Fig. 9(b)). The results indicate that capacitors with smaller capacitance exhibit faster charging rates when the harvester is working in the same vibrational mode. Specifically, under the 1st order bending mode, the 47 μF capacitor reaches a saturation voltage of 8.06 V within approximately 80 s, whereas the 470 μF capacitor reaches only 2.86 V after 120 s. Moreover, the harvester demonstrates superior charging performance in the 2nd order bending mode, achieving a significantly higher saturation voltage of 21.22 V within a shorter time (approximately 45 s) for the 47 μF capacitor, compared to its performance in the 1st order bending mode.

The performance of the proposed 3π/4 configuration is further tested by lighting the "UoA" LED array comprising 24 green LEDs connected in parallel. As illustrated in Fig. 9(a), a 220 μF capacitor (C_2) is connected in parallel with the LED array to smooth the rectified voltage. Each LED has a rated voltage of approximately 2 V, and the harvester's output voltage stabilized at different levels depending on the activated bending mode, as shown in Fig. 9(c). In the 1st order bending mode, the rectified voltage stabilizes at 1.93 V and lights up the LED array after a charging period of 40.5 s once S_2 is switched on (see Supplementary Video S4). By contrast, when operating under the 2nd order bending mode, the harvester achieves a higher stabilized voltage of 2.01 V and lights the LED array within only 8.6 s (see Supplementary Video S5). This higher stabilized voltage, combined with the shorter charging time, highlights the superior energy conversion efficiency of the proposed configuration when operating in the 2nd order bending mode.

The performance of the proposed configuration is further evaluated by powering a low-power wireless temperature sensor. As shown in Fig. 9(a), a 470 μF capacitor (C_3) is connected in parallel with the sensors to stabilize the terminal voltage and store the harvested energy. Based on the terminal voltage variation in Fig. 9(d) and the experiment (see Supplementary Video S6), the VIV-ABPEH with a central angle of 3π/4 charged C_3 from 0 V to 5.04 V within 279.8 s, after which the sensor is successfully activated ("sensor on"). Then, wind excitation is stopped, and the stored energy in C_3 sustained sensor operation for an additional 35.4 s. Each signal transmission from the temperature sensor caused a voltage drop of approximately 0.029 V in 1 s, enabling 35 successful transmissions, as shown in Fig. 9(d) and (f). Overall, the 3π/4 configuration demonstrated the capability of powering the temperature sensor for 35.4 s after 279.8 s of excitation in the 1st order bending mode. By contrast, as shown in Fig. 9(e) and the experiment (see Supplementary Video S7), the same configuration charged C_3 to 5.04 V within 60.0 s in the 2nd order bending mode, after which the sensor is activated and transmits temperature signals 35 times within 35.3 s. These results indicate that, compared to the 1st order bending mode, the 2nd order bending mode provides substantially improved charging efficiency while maintaining an equivalent level of sensor operation.

4. Conclusions

This paper proposes a VIV-based arch beam piezoelectric energy harvester (VIV-ABPEH) and presents a comprehensive investigation of the influence of arch beam curvature on its performance in varying incident wind directions. Finite element analysis is employed to predict the natural frequencies of the first four modes of both the conventional VIV-based straight beam piezoelectric energy harvester (VIV-SBPEH) and the proposed VIV-ABPEH with central angles of π/4, π/2, 3π/4, and π. Wind tunnel experiments are conducted to systematically and comparatively evaluate the performances of the VIV-SBPEH and VIV-ABPEHs in terms of cut-in wind speed, lock-in wind speed range, mode activation, incident wind direction range, and electrical output. The main conclusions drawn from this study are summarized as follows:

- The VIV-ABPEHs with π/2 and 3π/4 configurations can capture wind energy across multiple lock-in wind speed ranges by activating higher-order vibration modes.
- The VIV-ABPEHs exhibit superior adaptability to incident wind direction compared with the conventional VIV-SBPEH.
- Activation of the 2nd order bending mode enables the proposed VIV-ABPEH to achieve substantially higher electrical output than that in the 1st order mode, though it entails a higher cut-in wind speed.
- The VIV-ABPEH with a 3π/4 configuration achieves superior overall performance, with the self-powered sensors operating more efficiently when the 2nd order bending mode is activated.

The proposed VIV-ABPEH provides a promising approach for supplying continuous power to sensor networks, particularly in remote or hard-to-access environments. Although multi-directional wind energy harvesting has been demonstrated through finite element analysis and experimental validation, several challenges remain. These include the relatively high cut-in wind speed required to activate the 2nd order bending mode, the influence of geometric scaling on energy harvesting efficiency, and the absence of a predictive theoretical model for power output. Further research is therefore required to reduce the cut-in wind speed, enhance power density, and establish a theoretical framework for performance prediction, thereby improving the robustness and reliability of VIV-based wind energy harvesting in diverse natural wind conditions.

CRediT authorship contribution statement

Cuipeng Xia: Writing – review & editing, Writing – original draft, Software, Methodology, Investigation, Formal analysis, Data curation, Conceptualization. **Lihua Tang:** Writing – review & editing, Supervision, Methodology, Investigation. **Tianle Meng:** Data curation. **Yawei Wang:** Investigation. **Huaijun Li:** Investigation. **Peilun Yin:** Writing – review & editing, Data curation. **Wan Sun:** Writing – review & editing, Investigation. **Weiqun Liu:** Writing – review & editing, Methodology. **Guobiao Hu:** Writing – review & editing, Methodology. **Kean C. Aw:** Writing – review & editing, Supervision, Investigation.

Declaration of competing interest

The authors declare that they have no known competing financial interests or personal relationships that could have appeared to influence the work reported in this paper.

Acknowledgments

This work was financially supported by a PhD scholarship from the China Scholarship Council (No. 202207000016).

Appendix A. Supplementary data

Supplementary data to this article can be found online at https://doi.org/10.1016/j.energy.2026.140251.

Data availability

All data that support the findings of this study are available within the article upon reasonable request.

References

[1] Li Y, Li Y, Wang Y, Xiao M, Tang H, Zi Y, Wang J, Li X, Liao W-H, Hu G. From nature's deadly strike to safety protection: mantis shrimp-inspired ultrafast energy transformation for smart surveillance, device. 2025.
[2] Wong CJ, Ee ZY, Tan YY, Sia TS, Woo Q, Lukman J, Ong LZQ, Koay JSC, Aw KC, Gan WC, Tan ST. Dynamic real-time monitoring of microalgal photosynthesis using droplet triboelectric nanogenerators. Adv Funct Mater 2025.
[3] Wang Y, Du H, Yang H, Xi Z, Zhao C, Qian Z, Chuai X, Peng X, Yu H, Zhang Y, Li X, Hu G, Wang H, Xu M. A rolling-mode triboelectric nanogenerator with multi-tunnel grating electrodes and opposite-charge-enhancement for wave energy harvesting. Nat Commun 2024;15:6834.
[4] Sun W, Wang Y, Liu Y, Su B, Guo T, Cheng G, Zhang Z, Ding J, Seok J. Navigating the future of flow-induced vibration-based piezoelectric energy harvesting. Renew Sustain Energy Rev 2024;201.
[5] Zhang D, Zhang X, Yin P, Xia C, Tan P. Performance enhancement of piezoelectric energy harvesters based on flow-induced vibration via bio-inspired design. Phys Fluids 2025;37.
[6] Li Y, Ma X, Tang T, Zha F, Chen Z, Liu H, Sun L. High-efficient built-in wave energy harvesting technology: from laboratory to open ocean test. Appl Energy 2022;322.
[7] Everett J, Sorokin V, Whittaker C, Aw K. Numerical and experimental analysis of the power output performance of a point absorber WEC for nearshore wave conditions. Ocean Eng 2024;309.
[8] Zhang D, Zhang X, Tan P, Li S, Yin P. Exploring the influence of concave-convex surface modifications on piezoelectric wind energy harvesting: a numerical analysis. Ocean Eng 2024;311.
[9] Xia C, Yang J, Tang L, Yin P, Li Z, Wang B, Aw KC. A multi-directional and multi-modal galloping piezoelectric energy harvester with tri-section beam. Smart Mater Struct 2024;33.
[10] Cui Y, Luo H, Yang T, Qin W, Jing X. Bio-inspired structures for energy harvesting self-powered sensing and smart monitoring. Mech Syst Signal Process 2025;228.
[11] Shrestha K, Deo A, Teli A, Bhatta T, Park JY. A fidget spinner-inspired hybrid breeze wind energy harvester for self-sustainable wireless environmental monitoring system. Energy Convers Manag 2025:333.
[12] Xu Q, Long H, Tian S, Cheng Q, Liu J, Li M, Xie S, Wang P, Gao M, Sun Y. Dual-mode arrayed vibration-wind piezoelectric energy harvester. Energy Convers Manag 2025;324.
[13] Xue X, Xiang H, Ci Y, Wang J. A sustainable galloping piezoelectric energy harvesting wind barrier for power generation on railway bridges. Energy 2025;320.
[14] Xia C, Tang L, Wu Y, Hu G, Yin P, Aw KC, Inman DJ. Modeling and validation of a tri-section beam based multi-directional galloping energy harvester. Mech Syst Signal Process 2025;226.
[15] Yin P, Tang L, Li Z, Xia C, Li Z, Aw KC. Harnessing ultra-low-frequency vibration energy by a rolling-swing electromagnetic energy harvester with counter-rotations. Appl Energy 2025;377.
[16] Yin P, Han H, Tang L, Tan X, Guo M, Xia C, Aw KC. Kresling origami-inspired electromagnetic energy harvester with reversible nonlinearity. Smart Mater Struct 2024;33.
[17] Li Z, Ee Z, Pickett W, Patel B, Gan WC, Tang L, Su Y, Xia C, Yin P, Aw KC. A compliant mechanism actuated bistable hybrid mode triboelectric nanogenerator. Smart Mater Struct 2024;33.
[18] Maamoun AA, Esawi AMK, Mahmoud AA, Naeim DM, Arafa M. Waste-to-energy: repurposing flexible polyurethane waste for triboelectric nanogenerator applications. Appl Energy 2025;377.
[19] Yin P, Tang L, Aw KC, Xia C, Salman M, Zhang D, Peng Y, Li Z. Self-charge pumping circuit with high reverse-voltage diodes for stepwise charge enhancement in stack triboelectric nanogenerators. Energy Convers Manag 2026;347.
[20] Xu C, Wang CH, Peng S, Zhao L. Integrating synchronized charge extraction circuit with monostable and bistable metastructures for simultaneously enhanced vibration suppression and energy harvesting. Mech Syst Signal Process 2025;225.
[21] Li Q, He L, Lv X, Liu Z, Li Z, Fan W. A piezoelectric energy harvester based on center of gravity shift. Appl Energy 2025;377.
[22] Tang B, Fan X, Wang J, Yang H, Bai R, Yu X, Tan W. Energy harvesting of unequal-height cylindrical FIV considering wind direction. Int J Mech Sci 2025;290.
[23] Zhang H, Chen S, Karimi M, Li B, Saydam S, Hassan M. VIV–galloping coupled piezoelectric wind energy harvester for industrial applications. Int J Mech Sci 2025;302.
[24] Zhang Z, Lin S, Gu Y, Zhang L, Wang S, Zhai S, Kan J. Design and characteristic analysis of a novel deformation-controllable piezoelectric vibration energy harvester for low frequency. Energy Convers Manag 2023;286.
[25] Yu H, Fan L, Shan X, Zhang X, Zhang X, Hou C, Xie T. A novel multimodal piezoelectric energy harvester with rotating-DOF for low-frequency vibration. Energy Convers Manag 2023;287.
[26] Chen K, Gao Q, Fang S, Zou D, Yang Z, Liao W-H. An auxetic nonlinear piezoelectric energy harvester for enhancing efficiency and bandwidth. Appl Energy 2021;298.
[27] Tabatabaei-Nejhad SZ, Malekzadeh P, Eghtesad M. Out-of-plane vibration of laminated FG-GPLRC curved beams with piezoelectric layers. Thin-Walled Struct 2020;150.
[28] Shan X, Tian H, Chen D, Xie T. A curved panel energy harvester for aeroelastic vibration. Appl Energy 2019;249:58–66.
[29] Wang B, Li Z, Yang Z. A distributed-parameter electromechanical coupling model for a piezoelectric energy harvester with variable curvature. Smart Mater Struct 2020;29.
[30] Zhou Y, Nyberg TR, Xiong G, Zhou H, Li S. Precise deflection analysis of laminated piezoelectric curved beam. J Intell Mater Syst Struct 2016;27:2179–98.
[31] Jung W-S, Lee M-J, Kang M-G, Moon HG, Yoon S-J, Baek S-H, Kang C-Y. Powerful curved piezoelectric generator for wearable applications. Nano Energy 2015;13:174–81.
[32] Yang Z, Wang YQ, Zuo L, Zu J. Introducing arc-shaped piezoelectric elements into energy harvesters. Energy Convers Manag 2017;148:260–6.
[33] Zhou W, Wang B, Lim CW, Yang Z. A distributed-parameter electromechanical coupling model for a segmented arc-shaped piezoelectric energy harvester. Mech Syst Signal Process 2021;146.
[34] Liu S, Sun Y, Yang J. Design and simulation of a novel leaf-shaped piezoelectric energy harvester. Eng Res Express 2025:7.
[35] Thai TQ, Zhuang X, Rabczuk T. Curved flexoelectric and piezoelectric micro-beams for nonlinear vibration analysis of energy harvesting. Int J Solid Struct 2023;264.
[36] Wang F, Wang Z, Soroush M, Abedini A. Energy harvesting efficiency optimization via varying the radius of curvature of a piezoelectric THUNDER. Smart Mater Struct 2016;25.
[37] Mortazavi N, Ziaei-Rad S. Energy harvesting from vibrations of a beam under mass passage by arc-shaped auxetic cantilever beams. Eur J Mech Solid 2025;109.
[38] Shang M, Qin W, Li H, Liu Q, Wang H. Harvesting vibration energy by novel piezoelectric structure with arc-shaped branches. Mech Syst Signal Process 2023;200.
[39] Zhang X, Zhu F, Chen L, Chen X, Guo Y, Xu H. Dynamic characteristics and experimental research of linear-arch Bi-Stable piezoelectric energy harvester. Micromachines (Basel) 2022;13.
[40] Chen X, Zhang X, Guo Y, Zhu F. Modeling and performance analysis of a curve-shaped based doubly clamped piezoelectric energy harvester (CD-PEH). J Intell Mater Syst Struct 2023;35:3–16.
[41] Chen X, Zhang X, Wang L, Chen L. An arch-linear composed beam piezoelectric energy harvester with magnetic coupling: design, modeling and dynamic analysis. J Sound Vib 2021;513.
[42] He C, Lin S, Liu M, Zhang L, Kan J, Meng F, Zhang Z. A low-frequency unidirectional-strain-mode bistable piezoelectric vibration energy harvester via prestressing curved vibrators. Mech Syst Signal Process 2025;232.
[43] Hu Y, Yang B, Chen X, Wang X, Liu J. Modeling and experimental study of a piezoelectric energy harvester from vortex shedding-induced vibration. Energy Convers Manag 2018;162:145–58.
[44] Li Z, Lyu W, Gong C, Zhou S, Cheng L. Experimental investigation and dynamic analysis of a novel electromagnetic energy harvester based on airfoil flutter. Energy Convers Manag 2025;326.
[45] Wang K, Xia W, Ren J, Yu W, Feng H, Hu S. Wind energy harvesting inspired by Palm leaf flutter: observation, mechanism and experiment. Energy Convers Manag 2023;284.
[46] Li H, Zheng T, Ren H, Shen H, Diao B, Han W, Qin W, Yurchenko D, Ding H, Chen L. Improving piezoelectric wind energy harvesting performance with snowflake-shaped bluff bodies. Int J Mech Sci 2025;294.
[47] Wang J, Xiang H, Jing H, Zhu Y, Zhang Z. Stochastic analysis for vortex-induced vibration piezoelectric energy harvesting in incoming wind turbulence. Appl Energy 2025;377.
[48] Zhang J, E S, Cai J, Wu M, Wu H. A hybrid piezo-dielectric energy harvester with internal impact effect in vortex-induced vibrations. Int J Mech Sci 2025;303.
[49] Gong Y, Shan X, Hu H, Xie T, Yang Z. Vortex-induced swing (VIS) motion for energy harvesters and flowmeters. Appl Phys Lett 2020;117.
[50] Xia B, Mei X, Wang J. Enhanced performance of piezoelectric energy harvester by installing symmetrical flexible splitter plates. Mech Syst Signal Process 2025;225.
[51] Lan C, Zhang Y, Wang S, Lu Y, Wang Y, Hu G. Enhancing galloping-based energy harvesting through expanded quasi-zero-stiffness region. Smart Mater Struct 2025;34.
[52] Xia C, Tang L, Meng T, Wang J, Yin P, Zhang D, Li Z, Aw KC. A V-shaped galloping piezoelectric energy harvester exploiting bending and torsional modes. Int J Mech Sci 2025;306.
[53] Li J, Wang X, Cheng G, Zhang Z, Sun W. High-efficiency bi-directional wind energy harvesting based on wake interactions in bluff body tandem configuration. Mech Syst Signal Process 2025;234.
[54] Wang J, Luo L, Zhang Y, Hu G. Synergistic analysis of a wake galloping piezoelectric energy harvester coupled with a DC interface circuit. Energy 2025;334.
[55] Tian H, Yurchenko D, Li Z, Guo J, Kang X, Wang J. Dumbbell-shaped piezoelectric energy harvesting from coupled vibrations. Int J Mech Sci 2024;281.
[56] Wang J, Zhang Y, Liu M, Hu G. Etching metasurfaces on bluff bodies for vortex-induced vibration energy harvesting. Int J Mech Sci 2023;242.
[57] Xia C, Tang L, Yin P, Aw KC. Multi-directional and multi-modal vortex-induced vibrations for wind energy harvesting. Appl Phys Lett 2024;125.
[58] Wei N, Zhang Z, Cheng G, Yang H, Hu Y, Wen J. Study of a vortex-induced vibration piezoelectric wind energy harvester based on the synergy of multi-degree-of-freedom technology and magnetic nonlinear technology. Mech Syst Signal Process 2024;214.
[59] Liu F, Sun F, Liu W, Wang T, Wang H, Wang X, Lim WH. On wind speed pattern and energy potential in China. Appl Energy 2019;236:867–76.
[60] Boddapati K, Arrieta AF. Structural multistability for multi-speed wind energy harvesting from vortex-induced vibrations. Smart Mater Struct 2024;33.
[61] Chen S, Wang CH, Zhao L. A two-degree-of-freedom aeroelastic energy harvesting system with coupled vortex-induced-vibration and wake galloping mechanisms. Appl Phys Lett 2023;122.
[62] Jia J, Shan X, Upadrashta D, Xie T, Yang Y, Song R. An asymmetric bending-torsional piezoelectric energy harvester at low wind speed. Energy 2020;198.

[63] Gong Y, Shan X, Luo X, Pan J, Xie T, Yang Z. Direction-adaptive energy harvesting with a guide wing under flow-induced oscillations. Energy 2019;187.
[64] Ding J, Huang C, Zeng Z, Chen Z. A conical spiral piezoelectric energy harvester with parallel beams for all-directional flow energy harvesting. Smart Mater Struct 2024;33.
[65] Meng XK, Lu Z, Dai HL, Abdelkefi A. Comparative experimental investigation and effectiveness of sphere- and cylinder-based piezoelectric energy harvesters. Smart Mater Struct 2021;30.
[66] Li S, He X, Li J, Feng Z, Yang X, Li J. An in-plane omnidirectional piezoelectric wind energy harvester based on vortex-induced vibration. Appl Phys Lett 2022; 120.
[67] Zhang L, He Y, Meng B, Dai H, Abdelkefi A, Wang L. Omnidirectional wind piezoelectric energy harvesting. J Phys Appl Phys 2023;56.
[68] Wang J, Hu G, Su Z, Li G, Zhao W, Tang L, Zhao L. A cross-coupled dual-beam for multi-directional energy harvesting from vortex induced vibrations. Smart Mater Struct 2019;28.
[69] Shi T, Hu G, Zou L, Song J, Kwok KCS. Performance of an omnidirectional piezoelectric wind energy harvester. Wind Energy 2021;24:1167–79.
[70] Su W-J, Lin W-Y. Design and analysis of a vortex-induced bi-directional piezoelectric energy harvester. Int J Mech Sci 2020;173.
[71] Li W, Wang G, Yang C, Yang X, Song R. An omnidirectional piezoelectric energy harvester coupling vortex-induced vibration and wake galloping. Smart Mater Struct 2025;34.
[72] Zhang B, Li B, Fu S, Ding W, Mao Z. Experimental investigation of the effect of high damping on the VIV energy converter near the free surface. Energy 2022;244.
[73] Li H, Bernitsas CC, Congpuong N, Bernitsas MM, Sun H. Experimental investigation on synergistic flow-induced oscillation of three rough tandem-cylinders in hydrokinetic energy conversion. Appl Energy 2024;359.
[74] Garcia EMH, Bernitsas MM. Effect of damping on variable added mass and lift of circular cylinders in vortex-induced vibrations. J Fluid Struct 2018;80:451–72.
[75] Wang Z, Fan D, Triantafyllou MS. Illuminating the complex role of the added mass during vortex induced vibration. Phys Fluids 2021;33.